PCCP

PAPER

View Article Online
View Journal

Cite this: DOI: 10.1039/c8cp04593c

Molecular thermodynamic modeling of a bilayer perforation in mixed catanionic surfactant systems†

Ksenia A. Emelyanova and Alexey I. Victorov *

Perforated bilayers play an essential role in biology and in surface science. Here, we extend the classical aggregation model of catanionic surfactant mixtures to describe perforations in a self-assembled bilayer in aqueous salt. The model predicts that changing solution salinity and anionic-to-cationic surfactant ratio may lead to the spontaneous formation of pores in the bilayer and to the assembly of a micellar network. We estimate the dimensions of an optimal pore as a function of solution salinity and aggregate composition and show that with an increase of concentration of the deficient surfactant in a catanionic mixture, both the diameter and the thickness of the optimal pore decrease. This decrease is stronger for pores enriched in surfactant having a longer tail than for the pores enriched in the oppositely charged surfactant with a shorter tail. Our model helps to quantify the driving forces for the formation of a pore in a catanionic bilayer and to understand its role. For the aqueous mixtures C_{16}TAB/SOS/NaBr and DTAB/SDS/NaBr, our predictions are in reasonable although not quantitative agreement with available cryo-TEM and SANS data. Predicted radii of perforations are in the range of those obtained from SANS data for perforated bilayer disks.

Received 19th July 2018,
Accepted 15th October 2018

DOI: 10.1039/c8cp04593c

rsc.li/pccp

Introduction

Bilayer pores are important because they play an essential role in biological membranes[1,2] and also because perforated bilayers often appear as an intermediate structure before a self-assembled nonperforated bilayer transforms into a network of wormlike micelles and aggregates of other shapes.[3–5]

The model of a pore having a toroidal rim has been proposed recently for bilayers composed of ionic amphiphiles.[6] The toroidal shape of the rim plays a key role in the mechanism of pore formation. The combination of two curvatures of the rim – the small negative curvature in the plane of the pore and the large positive curvature across the bilayer – leads to preferential electrostatic interactions in the rim relative to the planar geometry of a nonperforated bilayer that has the same area per molecule. This results in the spontaneous formation of pores or disintegration of a bilayer in a certain salinity window. This distinguishes the new model[6] from a previously known model of pores having a cylindrical inner surface[5] and a purely two-dimensional model[7,8] that may not suggest such a perforation mechanism.

Perforated bilayers have been detected and extensively studied using both SANS and cryo-TEM in mixed surfactant systems.[5,9–11] However, only individual surfactants have been considered in our previous work.[6] The goal of this study is to apply our model to aqueous mixtures of cationic and anionic surfactants with added salt and to compare model predictions with available experimental data. We show how a combination of surfactant molecular parameters, including the length of the tail and the size of the head, affects the predicted shape and size of aggregates in aqueous catanionic mixtures, which are dependent on the proportion of surfactants and salinity.

In the next section, we briefly outline the model and its modification for mixtures. Predicted results and limitations of the model are discussed in Section 3.

Theoretical basis

Fig. 1 shows the geometry of our model. The pore in a bilayer has a toroidal rim, as shown in Fig. 1A. When three such pores are close together, they form the so-called Y-shaped junction, a structural element connecting three semiinfinite cylindrical micelles, as shown in Fig. 1B.

Based on the classical molecular-thermodynamic model,[12–15] the standard free energy of aggregation (g) for an aggregate of any shape includes a number of contributions.

St. Petersburg State University, 7/9 Universitetskaya nab., 199034 St. Petersburg, Russia. E-mail: victorov_a@yahoo.com; Tel: +7 921 301 1178

† Electronic supplementary information (ESI) available. See DOI: 10.1039/c8cp04593c

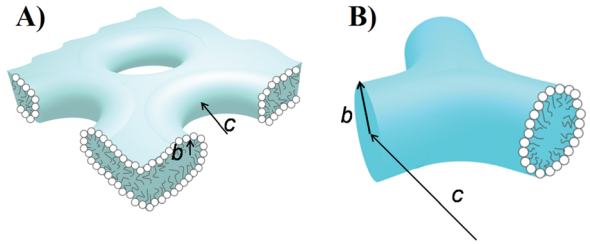

Fig. 1 (A) An element of a flat perforated bilayer with pores; (B) Y-shaped junction, an element of a network of branched cylindrical aggregates. b and c are the minor and major toroidal radii.

$$g = g_{hydr} + g_{def} + g_{int} + g_{st} + g_{ion} + g_{mix} \quad (1)$$

In this work, we use the expressions from the classical model of a surfactant mixture[13] for all contributions to the free energy, except for g_{ion} of the pore and the micellar junction, as explained below.

The major driving force of aggregation, the hydrophobic term g_{hydr}, is treated as independent of the aggregate shape. For a mixture of two surfactants, A and B, we have

$$g_{hydr} = \alpha_A g^A_{hydr} + \alpha_B g^B_{hydr} \quad (2)$$

where α_A and α_B are the mole fractions of surfactants A and B in the aggregate, respectively, and g^A_{hydr}, g^B_{hydr} are the free energies of transfer of their hydrophobic tails to the aggregate. The elastic deformation of surfactant tails in the interior of the aggregate is described by the deformational term

$$\frac{g_{def}}{kT} = B\frac{\pi^2}{80}\left(\frac{r_i}{l}\right)^2\left(\frac{\alpha_A}{N_A} + \frac{\alpha_B}{N_B}\right), \quad (3)$$

where r_i is a linear dimension of an aggregate, l is the Kuhn segment length, and N_A and N_B are the numbers of segments for surfactants A and B, respectively. B is a geometrical parameter that depends on the shape of the aggregate: $B = 3$ for a sphere, $B = 5$ for a cylinder and $B = 10$ for a planar bilayer. For a toroidal rim of a perforation, $B = (15\pi c - 12b)/(3\pi c - 4b)$ and $r_i = b$.[6,16]

The excess free energy of an interface between the aggregate core and the external solution is described by the interfacial term

$$g_{int} = \gamma(a - a_0) \quad (4)$$

where γ is the macroscopic interfacial tension between the hydrocarbon core and the surrounding bulk phase;[13] a is the average surface area per surfactant tail at the surface of the micellar core; $a_0 = l^2$ is the shielded area per surfactant molecule.

For the contribution from the steric repulsion between surfactant heads, we have

$$g_{st} = kT\ln\left(1 - \frac{a_p}{a}\right) \quad (5)$$

where a_p is the effective cross-sectional area of the surfactant heads. For mixtures, $a_p = \alpha_A a^A_p + \alpha_B a^B_p$, where a^A_p and a^B_p are the cross-sectional areas of the heads of the individual surfactants.

The free energy of mixing of surfactant tails in the core of the aggregate is estimated from the Flory–Huggins type of equation, as suggested by Nagarajan (eqn (78) and (79) of ref. 13).

The electrostatic contribution, g_{ion}, is obtained from the linearized Poisson–Boltzmann (LPB) equation for aggregates of different shapes. For the toroidal rim of the pore, we use an analytical approximation:[17]

$$\frac{g_{ion}}{kT} = t^2\frac{a\kappa_D}{8\pi l_B}\frac{K_p(x_0)}{K_{p+1}(x_0)} \quad (6)$$

where $t = \dfrac{4\pi l_B q}{e_0\kappa_D a}$ is the surface charge density in reduced units; q is the charge of the surface area a of the micellar surface; l_B is the Bjerrum length; e_0 is an elementary positive charge; κ_D is the inverse Debye length; $K_p(x_0)$ is the modified Bessel function of the 2nd kind of order p. The morphology flag p depends on the toroid's geometry:

$$p = \frac{m-1}{2}, \quad m = \frac{c - \sqrt{2}b}{c - \sqrt{2}b/2} \quad (7)$$

Eqn (6) reduces to previously known exact solutions of the LPB equation for spheres ($c \to 0$, $m = 2$), cylinders ($c \to \infty$, $m = 1$) and planes ($m = 0$).

The charge of a mixed surfactant aggregate is given by $q = \alpha_A q_A + \alpha_B q_B$, where q_A and q_B are the ionic charges of surfactants A and B, respectively. For a mixture of univalent cationic and anionic surfactants, we have $q = e_0|2\alpha_A - 1|$.

The free energy of the junction is estimated as

$$g_{jun} = \eta_{tor} g_{tor} + \eta_{pl} g_{pl}, \quad (8)$$

where g_{tor} and g_{pl} are the free energies of the toroidal and planar parts of the junction, and η_{tor} and η_{pl} are the volume fractions of these parts in the junction. The total surface area of the three toroidal parts of a junction and that of its planar part are $\pi b(\pi c - 2b)$ and $2c^2(\sqrt{3} - \pi/2)$, respectively; the volumes of these parts are $\pi b^2(\pi c/2 - 2b/3)$ and $2r_{pl}c^2(\sqrt{3} - \pi/2)$, where r_{pl} is the half thickness of a bilayer.

In this work, we consider aggregates of several shapes: spheres, cylinders, nonperforated lamellae, perforated lamellae and junctions. The optimal dimensions of an aggregate are found by minimizing its aggregation free energy. For minimization, we apply the polytope algorithm from the IMSL FORTRAN library.

The aggregate of stable shape possesses the lowest free energy. When cylinders are the most stable shape, they may be branched or nonbranched, depending on whether their spherical endcaps have lower free energy than the Y-junction or *vice versa*. The lowest free energy of a junction signifies the formation of a bicontinuous phase (even though within our model this 3-D structure is approximated by a combination of junctions that have a planar symmetry, see Fig. 1B).

Within our approach, a higher free energy of a nonperforated lamella than that of a toroidal rim of the pore reflects the tendency for spontaneous formation of pores leading eventually to the disintegration of a bilayer.

Results and discussion

To the best of our knowledge, the most detailed experimental studies of perforated structures have been performed for mixtures of cationic + anionic surfactants in aqueous solutions with added salt: cetyltrimethylammonium bromide + sodium octyl sulfate (C_{16}TAB/SOS/NaBr)[5] and dodecyltrimethylammonium bromide + sodium dodecyl sulfate (DTAB/SDS/NaBr).[11] Fig. 2 shows the chemical structure of the surfactant molecules.

Fig. 3A shows the free energy of aggregation calculated as a function of the average surface area per surfactant molecule for the C_{16}TAB/SOS system where the surfactant molar ratio is 70/30.

All model parameters, including the head cross-sectional areas of the surfactant for C_{16}TAB (a_p = 0.54 nm^2) and for SOS (a_p = 0.17 nm^2) have been taken from previous work.[13] The minima of the curves correspond to the optimal size of the aggregates of different shape. For a toroid, where the surface area depends on two linear dimensions, b and c, the curve is obtained for the optimal value of b and different values of c that correspond to the changing diameter of the pore in the bilayer. At a given salinity and surfactant ratio, a pore of a certain diameter has the lowest free energy, implying spontaneous perforation of a flat bilayer (lamella). Because the junctions have a lower free energy than cylindrical micelles, our model predicts stabilization of bicontinuous structures in the system. Fig. 3B shows a similar situation for the individual surfactant, C_{16}TAB, predicted from our model at a much higher salinity.

Comparison of Fig. 3B with Fig. 3A shows more than a tenfold increase in the energetic gap between lamellae and perforations for the mixture of surfactants. For the individual ionic surfactants, the predicted energetic gap between lamellae and perforations is very small and the salinity interval of stable perforations is extremely narrow.[6] This may explain why for individual ionic surfactants, perforated bilayer structures, to the best of our knowledge, have not yet been observed in experiment. However, for catanionic mixtures, flat perforated bilayers and perforated vesicles have been found by both SANS[5] and cryo-TEM studies.[5,9–11]

At the level of approximations of our model, the differences in free energies of competing structures shown in Fig. 3 are definitely too small (much less than kT) to give a reliable prediction of the stable aggregate morphology. The results from the model rather tell us that owing to thermal fluctuations, aggregates of different competing shapes are likely to appear in the shape transition regions. This is confirmed by many experimental TEM pictures where aggregates of different shapes are typically seen together.

As a major test of model predictions, we use the available experimental data on catanionic surfactant mixtures. Our calculations for C_{16}TAB/SOS/NaBr show that addition of SOS to C_{16}TAB-rich aggregates favors the appearance of pores by gradually increasing the energetic gap between the torus and the lamella; perforated structures are predicted at progressively lower salinities. This is the result of a partial compensation of charge in the catanionic aggregate. In contrast to individual surfactants, we predict perforated structures even in salt-free catanionic mixtures, in agreement with experiment.[5,11] Expectedly, the model describes a symmetrical behavior with respect to adding C_{16}TAB to a SOS-rich system.

Shown in Fig. 4 are predicted maps of stable aggregate morphologies in the aggregate composition–salinity plane for two catanionic mixtures. For both systems, our model gives two separate zones of stable perforated structures. Stable perforations are more energetically favorable at lower salinity than at higher salinity; the largest free energy gain is predicted for salt-free mixtures.

For systems enriched either in the cationic surfactant or in the anionic surfactant, addition of salt leads to the same sequence of shape transitions: spheres → cylinders (nonbranched → branched) → perforated bilayers → nonperforated bilayers (lamellae). Experimental phase diagrams for these systems[10,18] show similar sequences of aggregate shapes, although no experimental studies have been performed on perforated aggregates for solutions enriched in cationic surfactant.

For the DTAB/SDS/NaBr system, the lower part of the predicted diagram in Fig. 4A reflects the major trends observed in the cryo-TEM experiment:[11] (1) an increase of DTAB content results in a sequence of aggregates having progressively decreasing mean curvatures, including transitions from rodlike micelles to branched wormlike micelles, then to a network, perforated bilayers and, finally, to nonperforated bilayers; (2) an increase of salinity leads to stabilization of structures with smaller mean curvatures at a lower DTAB content.

Fig. 4 shows the location of perforated structures, as observed in experiment (flat bilayers and vesicles). Open symbols show the gross composition of experimental mixtures that certainly differs from the composition of the aggregates. For C_{16}TAB/SOS/NaBr, the aggregate's composition has been calculated[5] in the pseudophase approximation,[19] using the PB equation for curved aggregates to estimate the (dominant) electrostatic contribution to the interaction parameter β. These compositions are shown by black symbols in Fig. 4B. For a given anionic-to-cationic surfactant ratio in the system, Bergström *et al.*[5] obtained different estimates of the aggregate composition, depending on the total surfactant content in the system. We expect more accurate estimates of the aggregate composition at low salinity owing to the dominating role of the unscreened electrostatic interactions and less accurate estimates at high salinity (total surfactant content) where aggregation is largely controlled by the

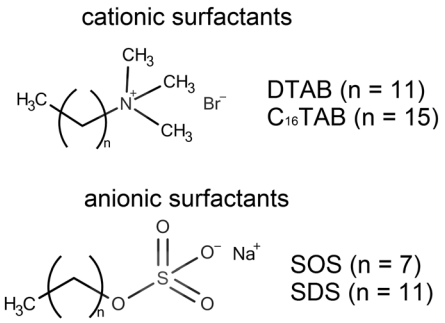

Fig. 2 Chemical structures of DTAB, C_{16}TAB, SDS and SOS.

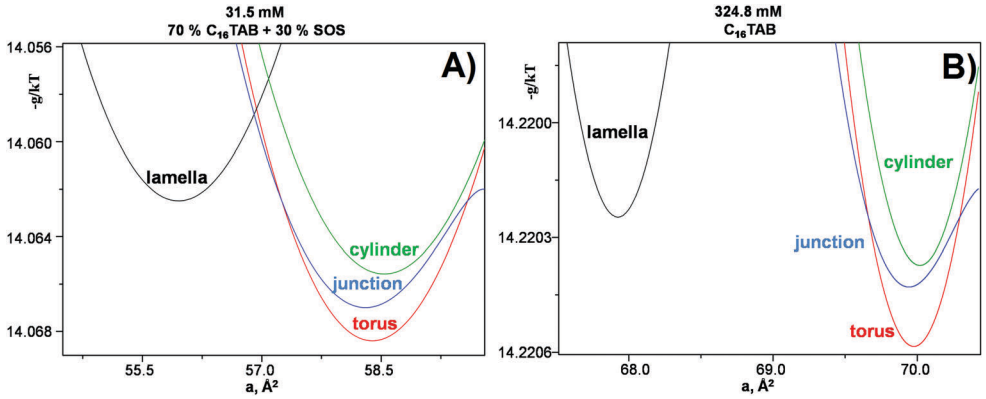

Fig. 3 Aggregation free energies for the nonperforated flat bilayer (lamella), the toroidal rim of a pore (torus), the cylindrical part of the micelle (cylinder) and the Y-shaped junction *vs.* the area per molecule at 298.15 K. (A) 70% C_{16}TAB + 30% SOS at 31.5 mM salt; (B) C_{16}TAB at 324.8 mM salt.

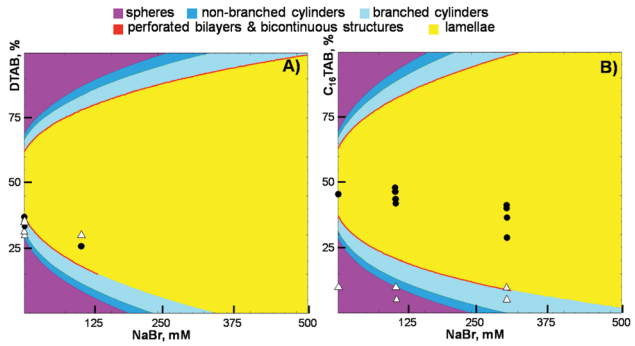

Fig. 4 Maps of stable aggregate morphologies for (A) DTAB/SDS/NaBr; (B) C_{16}TAB/SOS/NaBr aqueous mixtures at 298.15 K. Color: Thermodynamically stable shape predicted from the model. Symbols: Perforated structures from cryo-TEM studies on DTAB/SDS/NaBr[11] and from SANS studies on C_{16}TAB/SOS/NaBr;[5] shown are experimental gross compositions (open symbols) and aggregate compositions (black symbols) estimated using the pseudophase model, see the text.

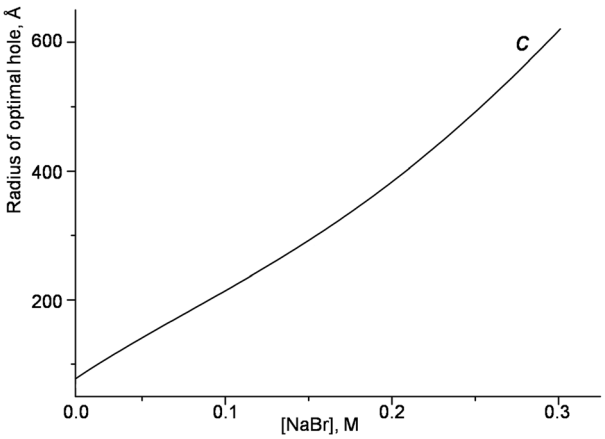

Fig. 5 Predicted radii of an optimal pore in the bilayer *vs.* solution salinity in the C_{16}TAB/SOS/NaBr aqueous mixture at 298.15 K.

specific chemistry of the surfactants and salt. Fig. 4B shows all these estimates even though our model in its present form may not reflect the effect of the total surfactant content on the characteristics of the aggregate. One zone of stable perforated structures predicted from our model falls in between the two sets of experimental points. Although there is no quantitative agreement with experiment, the model reflects correctly the general trend: increasing salinity leads to stabilization of perforations at lower C_{16}TAB contents in SOS-rich aggregates.

For DTAB/SDS/NaBr, we also applied the pseudophase approximation to estimate the aggregate composition (Fig. 4A) from the known value of the interaction parameter $\beta = -25.5$[20] and the experimental CMC-values,[21] see the ESI.† For perforated structures in DTAB/SDS/NaBr mixtures, Fig. 4A shows somewhat better agreement between the theory and experiment than that illustrated in Fig. 4B for C_{16}TAB/SOS/NaBr.

Fig. 5 shows the predicted radii of the bilayer pores that have the lowest possible free energy at a given solution salinity. The radius–salinity curve in this figure corresponds to the varying composition of the perforated bilayer, along the stability zone of perforations shown in the lower part of Fig. 4A. The diameter of the stable pore gradually increases with an increase of salinity and eventually becomes so large that the curvature of the pore's toroidal rim becomes insignificant. This means that at high enough salinity, the model predicts lamellar aggregates with semicylindrical edges rather than pores with a toroidal rim in a bilayer.

SANS data on the radii of pores in bilayer disks and perforated vesicles obtained for aqueous mixtures of C_{16}TAB/SOS/NaBr at 0.1 M and 0.3 M NaBr[5] reveal no obvious systematic trend with the change of solution salinity. These data show pore radii somewhere between 100 Å and 220 Å for flat disks and between 45 Å and 125 Å for the vesicles. For 0.1 M NaBr, our predicted radius of *ca.* 200 Å (Fig. 5) is in much better agreement with experiment for flat disks than for the vesicles, possibly because our model of a flat bilayer does not take into account the curvature imbalance of a vesicle. For salinities around 0.3 M, the radii from the model are approximately three times larger than those from experiment, implying that the perforated bilayer is close to disintegration either into separate lamellar aggregates with semicylindrical edges or into cylindrical micelles.

We applied the model to predict the effect of aggregate composition and the surfactant molecular parameters on the

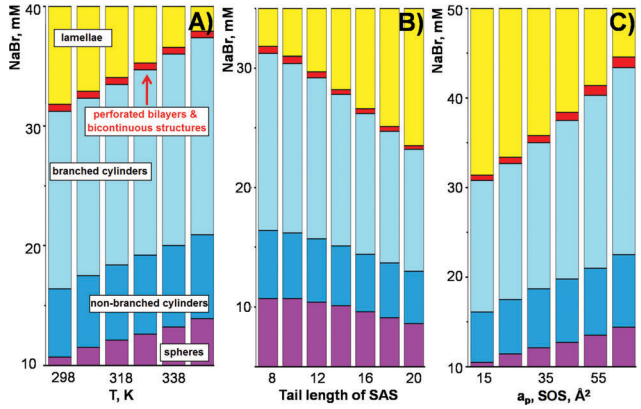

Fig. 6 Salinity intervals of stable shapes for catanionic aggregates containing 70 mol% C_{16}TAB. (A) Effect of temperature for C_{16}TAB/SOS/NaBr; (B) effect of the tail length of the anionic surfactant in C_{16}TAB/SAS/NaBr, T = 298 K; and (C) effect of the head cross-sectional area of an anionic surfactant having an octyl tail in the mixture with C_{16}TAB, T = 298 K.

evolution of the optimal dimensions of the pore's toroidal rim. Detailed results of calculations, including the discussion of the mechanism and driving forces for pore formation, are delegated to the ESI.† The dependence of parameter b on the aggregate composition is nontrivial with one maximum for the aggregates enriched in cationic surfactant and another maximum for the aggregates enriched in anionic surfactant.

The model predicts that upon increasing the concentration of the deficient surfactant in a catanionic mixture, both the diameter and the thickness of the stable pore may only decrease. This decrease is stronger for pores enriched in surfactant having a longer tail than for the pores enriched in the oppositely charged surfactant with a shorter tail. This asymmetry is more important at high salinity and less important at low salinity, where the behavior of the system is less surfactant-specific owing to the dominating weakly screened electrostatic interactions.

Fig. 6A shows the predicted effect of temperature on the aggregate shape in a C_{16}TAB/SOS/NaBr aqueous solution. An increase of temperature leads to the appearance of perforations at a higher salinity. An increase of the tail length of one of the surfactants narrows the salinity interval of stable perforations and shifts this interval to a lower salinity. An example is shown in Fig. 6B for different tails of sodium alkyl sulfates in C_{16}TAB/SAS/NaBr systems. An increase of the head cross-sectional area of the anionic or cationic surfactant leads to stabilization of perforations at a higher salinity and broadens the salinity interval, as shown in Fig. 6C.

Conclusions

The classical aggregation model of catanionic surfactant mixtures has been extended to describe perforations in a self-assembled bilayer in aqueous salt. The model predicts that changing solution salinity and anionic-to-cationic surfactant ratio may result in the spontaneous formation of pores in the bilayer that may finally reassemble into a spatial network of wormlike micelles. We show how the salinity windows of stable perforated structures systematically shift in response to a change in the length of the surfactant's tail or in the cross-sectional area of its head. Comparison of the calculated free energy increments that drive shape transitions shows that the propensity for forming bilayer pores is much stronger in mixtures of cationic and anionic surfactants than in the bilayers containing an individual ionic surfactant in aqueous salt. The model predicts that perforated structures may appear even in a salt-free surfactant mixture, in agreement with experiment.

We applied the model to predict how the dimensions of an optimal pore respond to a change of the aggregate's composition and of the surfactant molecular parameters. The model shows that with an increase of concentration of the deficient surfactant in a catanionic mixture, both the diameter and the thickness of the optimal pore may only decrease. This decrease is stronger for the pores enriched in surfactant having a longer tail than for the pores enriched in the oppositely charged surfactant with a shorter tail. This asymmetry is more important at high salinity and less important at low salinity, where the behavior of the system is less surfactant-specific owing to the dominating role of weakly screened electrostatic interactions.

For aqueous mixtures of C_{16}TAB/SOS/NaBr and DTAB/SDS/NaBr, our calculated results with no adjustable parameters are in reasonable although not quantitative agreement with the available cryo-TEM[11] and SANS results on perforated structures.[5] The predicted radii of perforations (*e.g.*, 200 Å at 0.1 M KBr) are in the range of those obtained from SANS studies for perforated bilayer disks.[5]

The model shows two separate zones of perforated bilayer structures in solutions rich either in cationic or in anionic surfactant. This seems to be in line with the observed phase diagrams for such systems,[10,18] however for solutions rich in cationic surfactant, to the best of our knowledge, there is no experiment on perforations.

Our model helps to explain the driving forces for the formation of a pore in a catanionic bilayer and to understand its role. Even though the performance of this simple model is mostly not quantitative, our predictions are important because they help to establish the expected response of the system to a change of composition and molecular characteristics of surfactants.

Definitely, there are a number of factors, including counterion condensation,[22] finite size[23] and specific chemistry of ions,[23–25] charge regulation,[26] *etc.* that all have an effect on the electrostatic contribution and hence may have an impact on the calculated results. With the simplified model of this work, we merely aimed to demonstrate that the sole interplay between the electrostatics and the deformation of hydrophobic tails suffices to explain and describe the formation of pores. Quantifying the contributions from different specific factors to the electrostatic term and studying their role in the formation of a bilayer pore are among the prospects for future work.

Conflicts of interest

There are no conflicts to declare.

Acknowledgements

We gratefully acknowledge the Russian Science Foundation (project # 16-13-10042) for financial support.

References

1 M. R. Lieber and T. L. Steck, *J. Biol. Chem.*, 1982, **257**, 11651.
2 H. Leontiadou, E. A. Mark and S.-J. Marrink, *Biophys. J.*, 2007, **92**, 4209.
3 D. Danino, *Curr. Opin. Colloid Interface Sci.*, 2012, **17**, 316.
4 M. Almgren, *Soft Matter*, 2010, **6**, 1383.
5 L. M. Bergström, S. Skoglund, K. Edwards, J. Eriksson and I. Grillo, *Langmuir*, 2014, **30**, 3928.
6 K. A. Emelyanova and A. I. Victorov, *Langmuir*, 2017, **33**, 13438.
7 M. D. Betterton and M. P. Brenner, *Phys. Rev. Lett.*, 1999, **82**, 1598.
8 M. Fošnarič, V. Kralj-Iglič, K. Bohinc, A. Iglič and S. J. May, *J. Phys. Chem. B*, 2003, **107**, 12519.
9 N. Kamenka, M. Chorro, Y. Talmon and R. Zana, *Colloids Surf.*, 1992, **67**, 213.
10 K. L. Herrington, E. W. Kaler, D. D. Miller, J. A. Zasadzinski and S. Chiruvolu, *J. Phys. Chem. B*, 1993, **97**, 13792.
11 R. Kakehashi, G. Karlsson and M. Almgren, *J. Colloid Interface Sci.*, 2009, **331**, 484.
12 R. Nagarajan and E. Ruckenstein, in *Equations of state for fluids and fluid mixtures*, ed. J. V. Sengers, R. F. Kayser, C. J. Peters and H. J. White, Elsevier Science, Amsterdam, 2000, pp. 589–749.
13 R. Nagarajan, in *Structure-performance relationships in surfactants*. ed. K. Esumi and M. Ueno, Marcel Dekker, Inc., NY-Basel, 2nd edn, 2003, pp. 2–110.
14 A. Shiloach and D. Blankschtein, *Langmuir*, 1998, **14**, 1618.
15 A. Goldsipe and D. Blankschtein, *Langmuir*, 2007, **23**, 5942.
16 A. I. Victorov, N. V. Plotnikov and P.-D. Hong, *J. Phys. Chem. B*, 2010, **114**, 8846.
17 V. A. Andreev and A. I. Victorov, *Mol. Phys.*, 2007, **105**, 239.
18 M. Bergström and J. S. Pedersen, *J. Phys. Chem. B*, 1999, **103**, 8502.
19 K. Holmberg, B. Jonsson, B. Kronberg and B. Lindman, *Mixed micelles*, John Willey & Sons, Ltd., 2002, ch. 5.
20 P. Holland, *ACS Symposium series, No. 501*, ed. P. M. Holland and D. N. Rubingh, American Chemical Society, Washington, DC, 1992, p. 41.
21 L. G. Chen and H. Bermudez, *Langmuir*, 2008, **29**, 2805.
22 V. Andreev and A. Victorov, *J. Chem. Phys.*, 2010, **132**, 054902.
23 S. Koroleva and A. Victorov, *Langmuir*, 2014, **30**, 3387.
24 S. Koroleva and A. Victorov, *Phys. Chem. Chem. Phys.*, 2014, **16**, 17422.
25 D. Ben-Yaakov, D. Andelman, D. Harries and R. Podgornik, *J. Phys.: Condens. Matter*, 2009, **21**, 424106.
26 T. Markovich, D. Andelman and R. Podgornik, *EPL*, 2017, **120**, 26001.

